J Biomol NMR (2007) 37:313–320
DOI 10.1007/s10858-007-9145-y

ARTICLE

Rapid and accurate processing method for amide proton exchange rate measurement in proteins

Harri Koskela · Outi Heikkinen · Ilkka Kilpeläinen · Sami Heikkinen

Received: 11 September 2006 / Accepted: 15 January 2007 / Published online: 14 February 2007
© Springer Science+Business Media B.V. 2007

Abstract Exchange between protein backbone amide hydrogen and water gives relevant information about solvent accessibility and protein secondary structure stability. NMR spectroscopy provides a convenient tool to study these dynamic processes with saturation transfer experiments. Processing of this type of NMR spectra has traditionally required peak integration followed by exponential fitting, which can be tedious with large data sets. We propose here a computer-aided method that applies inverse Laplace transform in the exchange rate measurement. With this approach, the determination of exchange rates can be automated, and reliable results can be acquired rapidly without a need for manual processing.

Keywords Exchange-resolved ^{15}N-HSQC · Gifa · Inverse Laplace transform · Protein backbone amide hydrogen exchange · Saturation transfer · Ubiquitin

Introduction

Protein is a dynamic entity, which interacts with surrounding media. The most important interaction, that molds the structure of protein itself, is with the solvating water molecules. The amide hydrogen exchange rates of a protein with surrounding water provides information on the stability of hydrogen bonding, details about tertiary structure, and protein-ligand interactions.

NMR spectroscopy is a convenient tool to study these dynamic processes. Several methods to observe amide hydrogen exchange have been published. These include diffusion and exchange line broadening measurements (Dempsey 2001), and also more sophisticated methods capable of suppressing possible NOE/ROE contributions from protons in close proximity (Hwang et al. 1997). However, possibly the most straightforward way is to measure saturation transfer of water magnetization to amide protons. In this method, water resonance is selectively saturated with a low-power RF pulse. Saturated water protons undergo chemical exchange with amide protons, causing their intensity to decay. The decay rate is dependent on the exchange rate (k_{ex}) and the longitudinal relaxation rate of amide proton (R_1). The decay of amide proton magnetization M_z can be expressed with the following equation (Wójcik et al. 1999)

$$M_z(t) = M_0\left[\frac{k_{ex}}{R_d}e^{-R_d t} + \frac{R_1}{R_d}\right] \quad (1)$$

where t is the duration of the low-power saturation pulse on water, and R_d is the apparent decay rate ($= R_1 + k_{ex}$). According to Eq. 1, when the saturation pulse duration t is zero, M_z equals the steady state magnetization M_0. When t approaches infinity, the magnetization will not decay to zero, but reaches a saturated state (M_{sat}) instead:

H. Koskela (✉)
Finnish Institute for Verification of the Chemical Weapons Convention (VERIFIN), University of Helsinki, P.O. Box 55, Helsinki 00014, Finland
e-mail: Harri.T.Koskela@helsinki.fi

O. Heikkinen · I. Kilpeläinen · S. Heikkinen
Laboratory of Organic Chemistry, University of Helsinki, P.O. Box 55, Helsinki 00014, Finland

$$\begin{aligned} M_z(0) &= M_0, \\ M_z(\infty) &= M_0 \frac{R_1}{R_d} = M_{sat} \end{aligned} \quad (2)$$

As can be seen from Eq. 2, the ratio of M_{sat} and M_0 equals to the ratio of R_1 and R_d. Using values M_{sat}, M_0 and R_d and we can calculate both R_1 and k_{ex}:

$$\begin{aligned} \frac{R_1}{R_d} &= \frac{M_{sat}}{M_0} \Rightarrow \\ R_1 &= \frac{M_{sat}}{M_0} \cdot R_d, \\ k_{ex} &= \left(1 - \frac{M_{sat}}{M_0}\right) \cdot R_d \end{aligned} \quad (3)$$

Conventional presaturation of water resonance has some limitations. With a very short presaturation pulse the spin populations on energy levels do not even out. Rather, the presaturation pulse will lead to a nutation of water magnetization to a fixed angle, and therefore giving usually a non-saturated spin state. This will cause non-linear fluctuations to the observed amide proton signal that undergoes exchange with water protons. Naturally, a higher presaturation power level can be used, but at the cost of selectivity. Leijon (1996) has proposed a convenient way to circumvent this problem. The modified saturation transfer experiment applies a selective 90° *y*-pulse on the water resonance to tilt it to *x*-axis. The magnetization is then maintained on the *x*-axis using a low-power spin lock with a duration of *t*. In this approach, the saturation state of water magnetization can be achieved rapidly without compromising selectivity. Furthermore, a field gradient pulse after the spin lock period will result in an efficient solvent suppression. However, when calculating the exchange rates, the effect of the selective excitation pulse must be taken into account. For this experiment, the ratio R_1/R_d can be calculated using Eq. 4 (Leijon 1996):

$$\frac{R_1}{R_d} = \frac{\frac{M'_{sat}}{M'_z(0)} \Delta M'_{sp}}{1 + \frac{M'_{sat}}{M'_z(0)} \left(\Delta M'_{sp} - 1\right)} \quad (4)$$

where $M'_z(0)$ is the amide proton magnetization when the spin lock duration t is zero, M'_{sat} is the amide proton magnetization when the spin lock duration t approaches infinity. The term $\Delta M'_{sp}$ is:

$$\Delta M'_{sp} = \frac{\pi^2 + 2\pi(R_d t_p) e^{R_d t_p} + 8(R_d t_p)^2}{\left(\pi^2 + 4(R_d t_p)^2\right) e^{R_d t_p}} \quad (5)$$

where t_p is the duration of the selective excitation pulse. The ratio R_1/R_d obtained from Eq. 4 can then be used in Eq. 3 to calculate R_1 and k_{ex}.

As exchange processes follow exponential behavior, apparent decay rates are traditionally extracted using mono-exponential curve fitting to the measured NMR signal intensities. However, exponential decay rates can also be evaluated using inverse Laplace transform (ILT), which is widely used in the diffusion spectroscopy (Johnson Jr 1999). As demonstrated in our previous study (Koskela et al. 2004) in evaluation of exponentially decaying relaxation data, the ILT processing utilizing Maximum Entropy Method (Delsuc and Malliavin 1998) offers a simple and robust way to evaluate exponential decay rates without prior knowledge of possible multi-exponential nature of data. The time-domain data with exponentially decaying intensities is transformed with ILT to a rate domain spectrum where the number of exponent components and decay rates can be evaluated. ILT is implemented to Gifa NMR processing software (Pons et al. 1996), where efficient macro-language gives tools to automate necessary processing steps, so that the complete evaluation of relaxation and exchange rates from NMR data can be performed with a single command. It should be noted that the use of ILT-method requires that intensity data follows exponentially decaying behavior. Therefore, it is not straightforward to combine ILT analysis and those sophisticated methods suppressing possible interference from NOE/ROE effects.

In the proposed exchange-resolved ^{15}N-HSQC experiment (Fig. 1), the saturation transfer period (Leijon 1996) is followed by amide proton detection with the sensitivity enhanced ^{15}N-HSQC (Palmer III et al. 1991). In the resulting spectrum, the amide cross peaks are separated by their ^{1}H and ^{15}N chemical shifts while their intensity decays with respect to the third, saturation transfer dimension (Fig. 2). The saturation transfer dimension is then processed with ILT to measure both R_1 and k_{ex} of each amide proton.

Materials and methods

NMR sample

Amide proton exchange rates were studied from uniformly ^{13}C,^{15}N-labeled human ubiquitin (Asla Biotech Ltd., Cat. Number UB06-nt). The solution contained 50 mM phosphate buffer (pH 6.0) in 10% D_2O / 90% H_2O with 0.05% NaN_3. The protein concentration was 1 mM in a 5 mm Wilmad 535-PP-7 NMR tube.

NMR experiments

The experiments were carried out using a Varian Unity Inova 500 NMR spectrometer equipped with a 5 mm

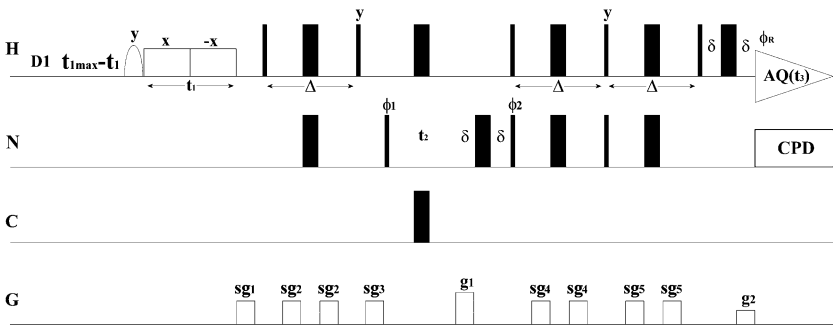

Fig. 1 Pulse sequence for exchange-resolved ^{15} N-HSQC. Narrow and wide filled bars denote 90° and 180° pulses, respectively. The 90° pulse widths were 6.9, 45, and 14.4 μs for ^{1}H, ^{15}N and ^{13}C, respectively. Unfilled bars denote pulsed field gradients with 1.0 ms duration and following strengths: sg_1–sg_5 = 4.0, 5.0, –15.0, 4.0, 4.0 G/cm and g_1–g_2 = 20, 2.02 G/cm. The unfilled half-ellipse denotes a selective 90° Gaussian excitation pulse (10.5 ms), and the unfilled rectangle represents a low-power spin lock (γB_1 = 111.35 Hz). The carbon channel pulse in the middle of t_2 is a hyperbolic secant inversion pulse. Pulses are along x-axis if not stated otherwise. Phase cycles are: $\varphi_1 = \{x, -x\}$, $\varphi_2 = \{x, x, -x, -x\}$, $\varphi_R = \{x, -x, -x, x\}$. The low-power spin lock pulse in the saturation transfer step is divided to two pulses with opposite phase and identical duration. The GARP decoupling (Shaka et al. 1985) is applied on ^{15}N during acquisition; the acquisition time was 8.5 ms. Delay Δ is the polarization transfer delay (5.37 ms), and δ corresponds to the total duration of the gradient pulse and the gradient recovery delay (1.1 ms). The relaxation time D1 was 1.0 s. The quadrature detection in the F_2 (^{15}N) dimension is accomplished with a gradient-based echo-antiecho selection. The axial peak displacement is achieved with the States–TPPI method (Marion et al. 1989) by inverting the phases φ_1 and φ_R on every second increment of t_2

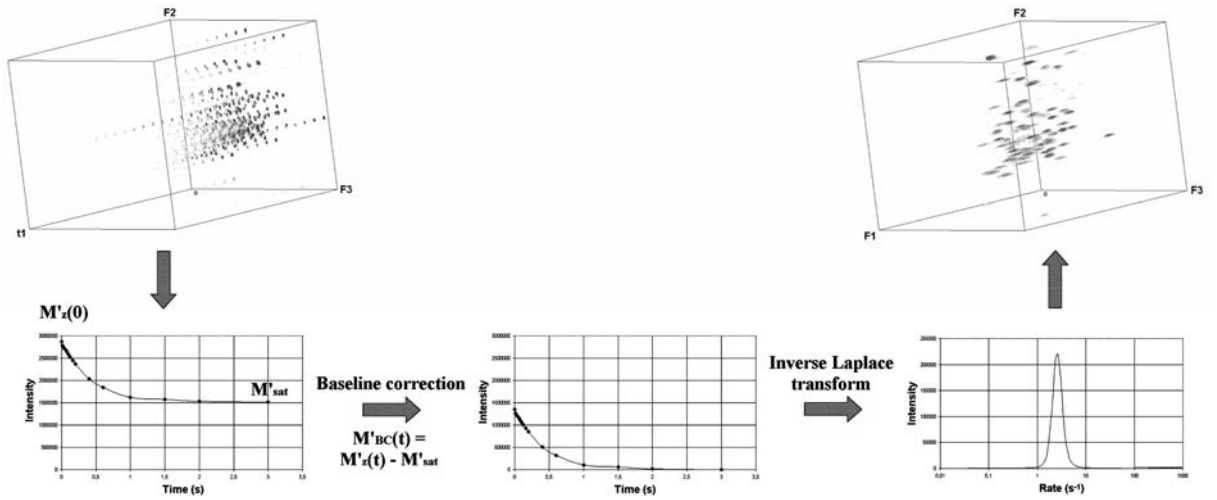

Fig. 2 ILT processing steps for saturation transfer data from the exchange-resolved ^{15}N-HSQC experiment. After 2D FT for the data matrix on F_3,F_2 dimensions the data matrix consists of ^{1}H,^{15}N -cross peaks which decay with respect to the t_1 dimension (on top left). The t_1 traces are extracted along the peak tops of the first ^{1}H,^{15}N-plane. The first step in the automated ILT processing is to extract $M'_z(0)$ and M'_{sat} for calculation of the ratio R_1/R_d according to Eq. 4. Next, the data is baseline (offset) corrected; without this step the non-zero end-intensity in the decay data would result in an infinitely slow exchange rate peak in the ILT spectrum. The third step, inverse Laplace transform, gives a rate domain spectrum with peak(s) at corresponding R_d's on a logarithmic scale. If needed, a true 3D spectrum can be formed with 2D FT-ILT processing (on top right), where peaks are separated by their ^{1}H,^{15}N chemical shifts and R_d rates. The results from the ILT processing are used to calculate R_1 and k_{ex}, which are saved to an output file

z-gradient triple-resonance (^{1}H,^{13}C,^{15}N) inverse probe head at 300 K. The spectrometer operating software was VNMR 6.1C (Varian Inc, Palo Alto, CA, USA). The exchange-resolved ^{15}N-HSQC spectrum was recorded with four scans per increment. The final data size was 18 × 128 × 683 real points, giving the total acquisition time of 20 h 55 min. The saturation time points t_1 (= t, Eq.1) were 0, 0.01, 0.02, 0.03, 0.04, 0.05, 0.06, 0.08, 0.1, 0.12, 0.16, 0.2, 0.4, 0.6, 1.0, 1.5, 2.0 and 3.0 s. Small saturation time increments were applied for the first saturation time points, and the increment size was increased gradually to ensure a time-efficient

and reliable exchange rate determination for amide protons experiencing exchange with various rates. Preliminary tests suggested R_d values of no slower than 1.6 s^{-1}. Therefore all amide protons should reach M'_{sat} intensities with spin lock duration t_1 of 3.0 s. The experiment was then repeated twice to examine precision of the method. For a quick confirmation of ^{1}H-^{15}N cross peak assignments a HNCA spectrum (Kay et al. 1990) was also measured.

Processing

The HNCA spectrum was processed in VNMR 6.1C, and subsequently imported to Sparky 3.110 NMR assignment software (Goddard and Kneller 2004) on a Linux workstation. The three exchange-resolved ^{15}N-HSQC spectra were processed with Gifa 4.4 NMR processing software (Pons et al. 1996) on a Silicon Graphics O2 workstation. The data was apodized on t_3 and t_2 dimensions (^{1}H and ^{15}N) using squared cosine window function. After 2D Fourier transform of ^{1}H,^{15}N dimensions, the final data matrix size was $18 \times 256 \times 1024$ real points. Before evaluation of exchange rates some prerequisites were performed. Automatic 2D peak picking was conducted on the first ($t_1 = 0$) ^{1}H,^{15}N plane to create a peak list file, and the noise level was extracted from an area without peaks. A file consisting of a list of t_1 time point values was created. According to the values in this t_1 list, proper δ_{min} and δ_{max} values for the ILT dimension were calculated by Gifa program. To determine the exchange rates automatically, a macro program was constructed. As an input for the macro program the duration of the water-selective excitation pulse used in the saturation transfer step (t_p) and the peak list name were given. The peak list was used to extract the t_1 traces one at the time for the ILT processing (Fig. 2). First, the maximum and minimum intensities of each peak's t_1 trace were used to calculate the $M'_{sat}/M'_z(0)$ ratio. Next, offset-correction was performed for the data, as without this step the non-zero end-intensity in the decay data would result in an infinitely slow exchange rate peak in the ILT spectrum. ILT with 100 spectral points and 400 iterations was computed for the data. R_d values were extracted from the rate domain spectrum using Gaussian lineshape fitting. The $M'_{sat}/M'_z(0)$ ratio, R_d and t_p were used to calculate R_1 and k_{ex} according to Eq. 3, 4 and 5, and finally the results for each amide proton were summarized to an output file, that could be exported to e.g., a spreadsheet software for further analysis. The total processing time of one spectrum with the macro program was under three minutes.

Results and discussion

In order to compare the accuracy of ILT using Maximum Entropy Method (Delsuc and Malliavin 1998) in evaluation of decay data, the t_1 trace intensity values from one exchange-resolved ^{15}N-HSQC spectrum of ^{13}C,^{15}N-labeled human ubiquitin were processed also with an exponential fitting. The intensity values of t_1 traces were imported to MS Excel (Microsoft Corporation, Redmond, WA, USA) spreadsheet software. The data was offset-corrected, and a mono-exponential curve fitting was performed with MS Excel's Solver routine utilizing GRG2 quasi-Newton non-linear regression algorithm (Lasdon et al. 1978; Fylstra et al. 1998) to extract R_d's. The R_d values obtained from ILT analysis were used to calculate corresponding decay curves. The quality of R_d's extracted with these two methods was tested by comparing how well the calculated data from the ILT and exponential fitting results explained the experimental data. The average of correlation coefficients (R^2) with the data shows a very good fit, $R^2 = 0.995$, for both methods. There is no major systematic deviation, as the average difference of the ILT results to the exponential fitting results is 0.7%, however, some differences between R_d's obtained with the ILT and exponential fitting can be observed (Fig. 3). Some of the largest deviations can be found from cases where the experimental data is difficult to fit if only a mono-exponential decay is presumed, like with the t_1 trace from T9 (Fig. 4). While the mono-exponential fitting for the data from the t_1 trace of T9 gave R_d of 19.40 s^{-1}, ILT evaluated the data to contain two components with R_d's 24.33 s^{-1} and 1.34 s^{-1}; the first of these components being the prominent one (Fig. 4A), and used for subsequent R_1 and k_{ex} calculation. A bi-exponential fitting gave also much better correspondence to the experimental data compared to a mono-exponential fitting, and with similar R_d results as ILT (Table 1). As ILT with Maximum Entropy Method (Delsuc and Malliavin 1998) does not need a prior knowledge of possible mono-/bi-/multi-exponentiality of the intensity decay data it can find the necessary number of exponential components, thus giving a good fit without need of manual intervention. If the deviation of the experimental data from mono-exponential decay curvature is due to noise, it can be naturally argued which one of the evaluated R_d's, the prominent component from the ILT spectrum or the mono-exponential fitting result, is the correct one. As the R^2 values are the same to the third decimal (Fig 4B), the decision is difficult to tell. On the other hand, if the data contains true multi-exponential decay, for example due to partial or complete overlapping of

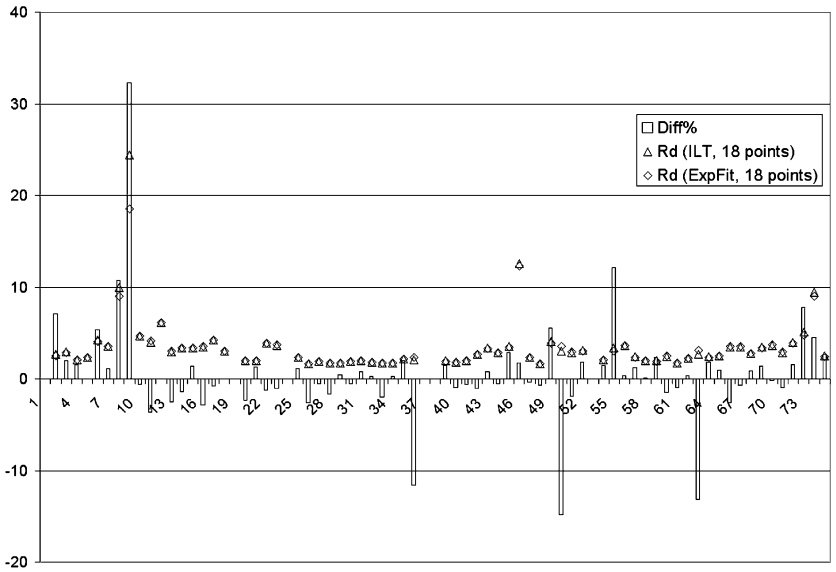

Fig. 3 Comparison of R_d values evaluated with ILT and exponential fitting with respect to the residue number. The unit for R_d is s^{-1}. The difference is shown as a percentage deviation of ILT results from corresponding exponential fitting results

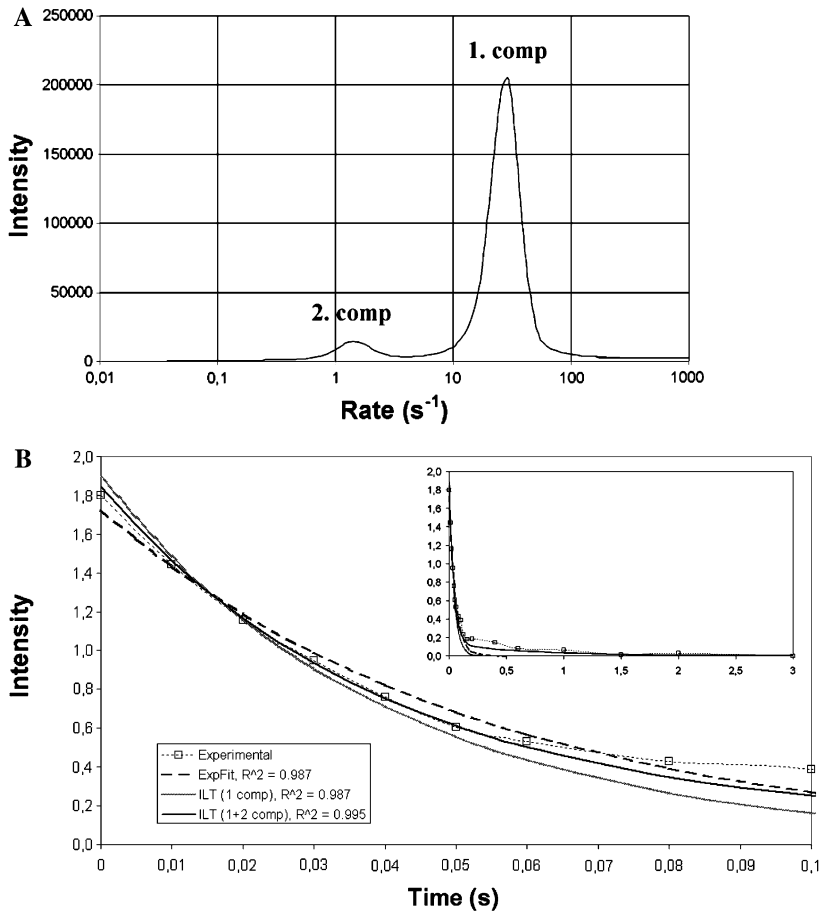

Fig. 4 Evaluations of t_1 trace intensity data along the peak T9 from one exchange-resolved ^{15}N-HSQC spectrum. (**A**) The ILT spectrum calculated with the proposed processing method indicates a bi-exponential characteristic in the data. (**B**) Correlation coefficient (R^2) between the experimental data and a mono-exponential fitting (ExpFit) curve is lower than between the experimental data and the calculated bi-exponential decay curve which uses both decay rate (R_d) values evaluated from the ILT analysis (1.+ 2. component). The calculated mono-exponential decay curve that uses the prominent component of ILT analysis (1. component) shows a little faster decay rate compared to exponential fitting (ExpFit) decay curve while correlation coefficients to the experimental data are identical

peaks, ILT can readily pinpoint this if the difference of decay rates is three-fold or larger (Jerschow and Müller 1998).

Acquisition of 18 experimental saturation transfer points for the exchange-resolved ^{15}N-HSQC spectrum requires a rather long, almost a full day of measurement time. Therefore, the reduction of the number of saturation time points to keep the total acquisition time of the spectrum moderate was also investigated. Total of eight points (t_1 = 0, 0.02, 0.05, 0.08, 0.16, 0.4,

Table 1 Decay rate evaluation results (R_d) from the t_1 trace of T9 with ILT, mono-exponential, and bi-exponential fitting, and the correlation coefficients (R^2) between the fitted curves and the experimental data

Method	R_d (1. comp)	R_d (2. comp)	R^2
ILT	24.33	1.34	0.995
ExpFit, mono-exponential	19.40	–	0.987
ExpFit, bi-exponential	26.15	1.45	0.998

Both exponential fittings were performed using a MS Excel's Solver routine utilizing GRG2 quasi-Newton non-linear regression algorithm. The first component is the more prominent of the two R_d's evaluated with ILT and bi-exponential fitting

1.5 and 3) from the original dataset were used for both ILT and exponential fitting. Using only eight saturation time points the total acquisition time would have reduced to less than 10 h. Correlation coefficients are again very good between experimental and calculated data, while exponential fitting shows a little better result (Average of R^2's were 0.995 and 0.994 for the exponential fitting and ILT, respectively). Average difference of the ILT results with respect to the exponential fitting is –3.0%, demonstrating a slight overall decrease in the ILT results. This systematic decrease of values is also evident when the ILT results calculated from eight points are compared to the ILT results from 18 experimental data points. The average difference is –2.9%, while the exponential fitting results with 8 experimental data points have an average difference of only 0.5% with respect to the exponential fitting results with 18 experimental data points. This is still a relatively small deviation, and can be in most cases accepted for practical purposes. Naturally, the acquisition parameters can be further revised, if the short total acquisition time is more important than the absolute accuracy of exchange rates, like in protein-ligand interaction screening where relative changes of amide proton exchange rates are the main interest.

The proposed ILT processing scheme uses $M'_{sat}/M'_z(0)$ ratios in calculation of R_1 and k_{ex} values. Therefore, it relies on the assumption that the duration of the last t_1 delay is sufficiently long to give M'_{sat} intensity for all peaks. If this is not the case, the estimated M'_{sat} will be too large. This may lead to a systematic error in calculation of the k_{ex} values. In order to trace possible systematic errors in the processing scheme, the t_1 trace intensity values from the exchange-resolved ^{15}N-HSQC spectra were analyzed also with full parameterization. The trace intensity values follow the equation (Leijon 1996):

$$M_z(t) = M_0\left[\left(\frac{k_{ex}}{R_d}e^{-R_d t_p} + \frac{k_{ex}e^{-R_d t_p} + \frac{\pi k_{ex}}{2R_d t_p}}{R_d\left(1 + \frac{\pi^2}{4(R_d t_p)^2}\right)}\right)e^{-R_d t} + \frac{R_1}{R_d}\right] \quad (6)$$

The equation describes the decay of single peak, and takes into account the effect of the water-selective excitation pulse. The fitting of the Eq. 6 to the experimental data with respect to M_0, k_{ex} and R_1 (while $R_d = R_1 + k_{ex}$) was done using Levenberg–Marquardt algorithm. This was performed in MS Excel software utilizing an add-on optimization software (Volpi 2006; Garcia and Volpi 2006). The obtained k_{ex} values were then compared to the k_{ex} values evaluated with the ILT processing. Fig. 5 shows that values from the ILT processing agree well with the Levenberg–Marquardt fitting results. The average difference of the ILT processing results to the Levenberg–Marquardt fitting results was 0.9 %, and does not indicate any major systematic deviation. The largest deviation is again observed for the residue T9, where the experimental data, based on the ILT analysis, showed distinct bi-exponential characteristics (see previous sections). Naturally, it is clear, that great care should be applied when choosing the duration for the last t_1 value (the longest saturation duration), as the selected value that has to satisfy the M'_{sat} condition for all peaks. For small to medium sized proteins the last t_1 value of 3–5 s should be sufficient.

The wealth of information obtainable from amide proton exchange rate data is clearly visible in Fig. 5. The amide proton exchange measurements can provide information on flexibility, solvent accessibility, as well as the secondary structure of proteins. As can be seen in Fig. 5, the amide protons in well-defined secondary structures, like α-helices and β-sheets, have low exchange rates due to hydrogen bonding. The highest rate values are observed for those amide protons that are exposed to water, like in turns and bends situated on the exterior of the tertiary structure. Correspondingly, if the tertiary structure of the protein hinders the exposure of residues, and offers additional possibilities for inter- or intramolecular hydrogen bonding, the amide proton exchange rates decrease. In cases where backbone hydrogen bonding has a crucial role in ligand binding (Nakamura et al. 2006) exchange rate analysis has potential to offer more detailed information about protein-ligand interaction.

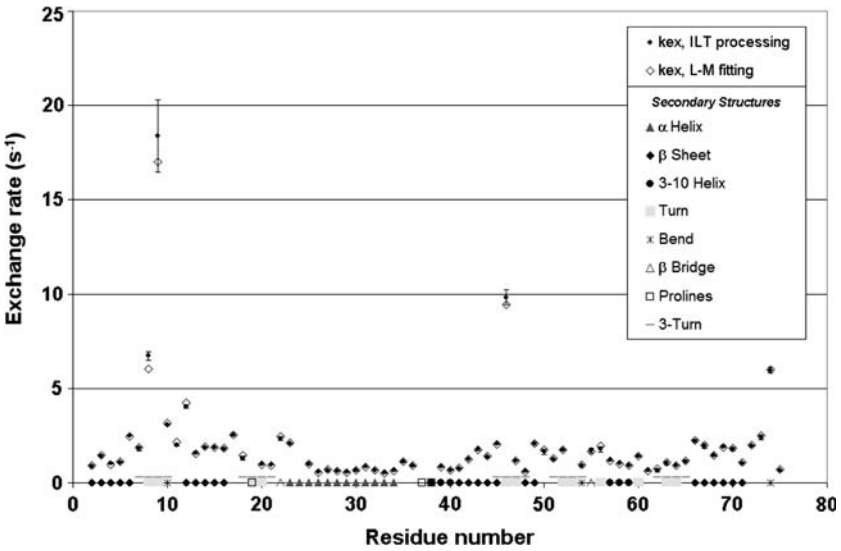

Fig. 5 Comparison of exchange rate (k_{ex}) results by the ILT processing and the Levenberg–Marquardt fitting from the exchange-resolved ^{15}N-HSQC data of ^{13}C,^{15}N-labeled ubiquitin. The exchange rates evaluated with the ILT processing are average values from the analysis of three separate spectra, and are plotted with error bars (standard deviation) as a function of the residue number. The exchange rates evaluated with the Levenberg–Marquardt fitting are results from the analysis of one spectrum. The secondary structure of ubiquitin (PDB accession code 1D3Z) according to DSSP (Kabsch and Sander 1983) is also included. The slow exchange is associated with more ordered secondary structural units, like helices and β-sheets, while higher exchange rates are found at turns and bends

Conclusions

We have demonstrated here the potential of the ILT approach in measurement of amide proton exchange rates. It is a simple and robust method which does not require prior knowledge of the exchange times, nor laborious ''2D integration-fitting'' procedures. The ILT processing can be readily automated, thus offering a fast computer-aided tool to evaluate e.g., protein-ligand interactions. This gives an advance in cases where a large number of samples are under study.

References

Delsuc MA, Malliavin TE (1998) Maximum entropy processing of DOSY NMR spectra. Anal Chem 70:2146–2148

Dempsey CE (2001) Hydrogen exchange in peptides and proteins using NMR spectroscopy. Prog NMR Spectrosc 39:135–170

Fylstra D, Lasdon L, Warren A, Watson J (1998) Design and use of the Microsoft Excel Solver. Interfaces 28:29–55

Garcia LIR, Volpi L (2006) Levenberg–Marquardt algorithm v14.04.2006, http://digilander.libero.it/foxes

Goddard TD, Kneller DG (2004) SPARKY 3. San Francisco, University of California,

Hwang T-L, Mori S, Shaka AJ, van Zijl PCM (1997) Application of Phase-Modulated CLEAN chemical EXchange spectroscopy (CLEANEX-PM) to detect water-protein proton exchange and intermolecular NOEs. J Am Chem Soc 119:6203–6204

Jerschow A, Müller N (1998) Diffusion-separated nuclear magnetic resonance spectroscopy of polymer mixtures. Macromolecules 31:6573–6578

Johnson CS Jr, (1999) Diffusion ordered nuclear magnetic resonance spectroscopy: principles and applications. Prog NMR Spectrosc 34:203–256

Kabsch W, Sander C (1983) Dictionary of protein secondary structure: pattern recognition of hydrogen-bonded and geometrical features. Biopolymers 22:2577–2637

Kay LE, Ikura M, Tschudin R, Bax A (1990) Three-dimensional triple-resonance NMR spectroscopy of isotopically enriched proteins. J Magn Reson 89:496–514

Koskela H, Kilpeläinen I, Heikkinen S (2004) Evaluation of protein ^{15}N relaxation times by inverse Laplace transformation. Magn Reson Chem 42:61–65

Lasdon LS, Waren AD, Jain A, Ratner M (1978) Design and testing of a generalized reduced gradient code for nonlinear programming. ACM Trans Math Softw 4:34–50

Leijon M (1996) Proton exchange rates measured by saturation transfer using delayed randomization of the solvent magnetization. J Magn Reson B112:181–185

Marion D, Ikura M, Tschudin R, Bax A (1989) Rapid recording of 2D NMR spectra without phase cycling: application to the study of hydrogen exchange in proteins. J Magn Reson 85:393–399

Nakamura F, Pudas R, Heikkinen O, Permi P, Kilpeläinen I, Munday AD, Hartwig JH, Stossel TP, Ylänne J (2006) The structure of the GPIb-filamin A complex. Blood 107:1925–1932

Palmer III AG, Cavanagh J, Wright PE, Rance M (1991) Sensitivity improvement in proton-detected two-dimensional heteronuclear correlation NMR spectroscopy. J Magn Reson 93:151–170

Pons LJ, Malliavin TE, Delsuc MA (1996) Gifa V. 4: a complete package for NMR data set processing. J Biomol NMR 8:445–452

Shaka AJ, Barker PB, Freeman R (1985) Experimental demonstration of wideband spin inversion. J Magn Reson 64:547–552

Volpi L (2006) Optimiz.xla v.2.0, http://digilander.libero.it/foxes

Wójcik J, Ruszczynska K, Zhukov I, Ejchart A (1999) NMR measurements of proton exchange between solvent and peptides and proteins. A Biochim Pol 46:651–663